Greyscale 2D nanograting fabrication by multistep nanoimprint lithography and ion beam etching

Janek Buhl (jabu@tf.uni-kiel.de)
Christian-Albrechts-Universitat zu Kiel https://orcid.org/0000-0001-6633-5741

Danbi Yoo
Helmholtz-Zentrum Berlin fur Materialien und Energie GmbH

Markus Köpke
Christian-Albrechts-Universitat zu Kiel

Martina Gerken
Christian-Albrechts-Universitat zu Kiel

Nano Express

Keywords: Nanoimprint Lithography, Ion beam etching, Greyscale lithography, Nanopattern fabrication, Periodic nanogratings, Photonic crystal slab, Indium tin oxide, Nanostructured OLEDs

Posted Date: September 15th, 2020

DOI: https://doi.org/10.21203/rs.3.rs-74242/v1

Abstract

The application of nanopatterned electrode materials is a promising method to improve the performance of thin-film optoelectronic devices such as organic light-emitting diodes and organic photovoltaics. Light coupling to active layers can be enhanced by employing individual nanopatterns specifically tailored to the device structure. During the development process typically a range of different nanopatterns need to be evaluated. Fabrication of each of these nanopatterns using electron-beam lithography is time and cost intensive, particularly for larger scale devices, due to the serial nature of electron beam writing. Here, we present a meth-od to generate nanopatterns of varying depth with different nanostructure designs from a single one-dimensional grating template structure with fixed grating depth. We employ multiple subsequent steps of UV nanoimprint lithography and ion beam etching to fabricate greyscale two-dimensional nanopatterns. After each imprint step, the imprint resist is cured and etched to maintain the structural conformity. In this work we present variable greyscale nanopatterning of the widely used electrode material indium tin oxide. We demonstrate the fabrication of periodic pillar-like nanostructures with different period lengths and heights in the two grating directions. The patterned films can be used either for immediate device fabrication or pattern reproduction by convention-al nanoimprint lithography. This parallel processing approach promises cost-efficient large-scale nanopattern variation for the device development process.

Introduction

The performance of thin-film optoelectronic devices, such as organic and perovskite light-emitting diodes (OLEDs) and organic photovoltaics (OPV), has been increasing steadily over the last decades[1–4]. Their efficiencies however are still limited by losses inherent to the device architecture. In a default device stack more than 80% of the light cannot be utilized because of coupling to substrate modes, waveguided modes in the active layers or plasmonic modes at metal interfaces[5–6]. Various methods to access the light trapped in these modes such as the application of high-index substrate materials or the addition of one or multiple extraction lenses have been proposed[7–8]. Another promising approach is the introduction of a periodic or aperiodic nanopattern to the interfaces in the layer stack[9–15]. The nanostructure reduces total internal reflection and enables the outcoupling of quasi-guided modes[16–17]. Additionally, charge carrier injection may benefit from local field enhancement effects at nanopatterned electrodes[18–19]. To achieve a significant increase in coupling efficiency, the geometrical dimensions of the employed nanopattern must be adjusted to the particular device design. Suitable parameters can be determined via simulation of the layer stack[20]. In an LED the maximum increase in outcoupling efficiency should match the emission maximum whereas the maximum increase in coupling to the active layer in a solar cell should coincide with the absorption peak. Aside from enhancing the overall efficiency, periodic nanopatterns also allow for directional coupling of selective wavelengths[21–22] and may facilitate nanoparticle alignment during device fabrication[23–24]. In order to comply with specific requirements for different device architectures, a process to generate nanopatterned electrode films for device development must enable the creation of different shapes and pattern designs with adjustable structural

heights. This effectively requires a highly-controllable greyscale patterning method. Even though multiple greyscale electron beam lithography (EBL) techniques have been developed[25–28], they are usually complex, time-consuming and not suitable for large-scale patterning. Nanoimprint lithography (NIL) on the other hand is a low-cost process allowing for high-throughput reproduction of multiscale patterns[29]. However, the obtainable nanopatterns are essentially restricted to the geometrical shape and dimensions of the imprint template[30–31]. In this work we present a manufacturing method to introduce nanopatterns of variable shape and height into a transparent conductive indium tin oxide (ITO) film on a glass substrate. As ITO is the most commonly used electrode material for thin film optoelectronics, the resulting samples can be directly used for device fabrication. Additionally, they may also be utilized as imprint templates for simple reproduction of the generated pattern by NIL. We are able to create arbitrary two-dimensional greyscale patterns by performing multiple successive nanoimprint steps employing the same or different template patterns in each step. In contrast to other works applying multiple nanoimprint steps to achieve multi-dimensional patterns[32], we cure and etch the imprint resist after each imprint step. In doing so, we are able to maintain structural conformity to the desired pattern and to obtain greyscale features.

Experimental

The different stages of the nanopatterning process are depicted in Fig. 1. One or more initial master templates patterned by electron beam lithography, laser interference lithography, or other techniques are required as a basis for the resulting nanopattern. We used commercially available glass templates holding periodic one-dimensional nanogratings with period lengths ranging from 400 to 600 nm and a grating height of 140 nm. From the master templates we reproduced negative imprint templates from polydimethylsiloxane (PDMS), which we applied for up to three successive imprints. Subsequently, we employed a standard UV nanoimprint process described previously to impress the positive pattern into an imprint resist layer[33]. Patterning was performed on ITO coated glass substrates (Lumtec, specified ITO layer thickness 140 nm ± 20 nm). We chose the UV-curable imprint resist Amonil MMS4 (Amo GmbH), which is an organic-inorganic composite containing zirconium alkoxides. After reproduction of the one-dimensional pattern in the resist, we transferred the structure into the ITO layer by ion beam etching (IBE) using an IBE system PC3000 (Oxford Instruments). We employed a purely physical ion etching technique using only argon (Ar) plasma as the etchant in order to achieve a highly anisotropic etching. Choosing an RF power of 500 W and a beam current of 350 mA at a gas pressure of 8 torr allowed for a precisely controllable etching process while maintaining reasonable processing time. Following the pattern transfer we removed any residues of the imprint resist with tetramethylammonium hydroxide using a commercial photoresist stripper (TechniStrip P1316, MicroChemicals). By repeating the imprint and etching process rotating the imprint template by an angle for each imprint step we obtained two-dimensional greyscale patterns in the ITO.

Results And Discussion

The maximum structural depth for the first etching step is determined by the height of the imprint template and the etching rate ratio between the imprint resist and the ITO layer. To perform an etching rate analysis at the chosen etching parameters, we prepared several planar samples with and without the imprint resist. We etched partially masked samples for different times before measuring the resulting height difference with a profilometer. The measurements shown in Fig. 2 indicate constant etching rates over the entire process duration corresponding to an etching rate ratio of 1.2. Despite the low selectivity of the etching process (which is expected for a purely physical etching), it is suitable to transfer the grating pattern into the underlying ITO layer. However, as the ITO etching rate is lower than the etching rate of the imprint resist the maximum structural depth possible is only 116 nm (83% of the height of the imprint template).

The actual etching time for each sample was chosen according to the desired etching depth assuming the etching rates presented before. In order to account for potential thickness variations of the imprint resist during deposition, the etching process was additionally tracked in-situ by time-of-flight secondary ion mass spectrometry (TOF-SIMS), as shown in Fig. 3. Since the imprint resist contains zirconium (Zr), one can qualitatively track the presence of resist on the sample surface by monitoring the Zr content in the secondary ion gas mixture. While etching a planar sample, the Zr count decreases sharply after approximately 7 minutes indicating complete removal of the imprint resist and exposure of the ITO layer underneath. At the same time the indium (In) count rises abruptly corresponding to the beginning of the ITO etching. After a total etching time of 15 minutes the ITO count declines again indicating that the ITO layer is entirely removed. The sudden increase of the Si count at this point can be attributed to the etching of a 20 nm thick SiO_2 passivation layer underneath the ITO coating. Considering the etching durations for planar layers of the imprint resist (approx. 200 nm) and the ITO coating (140 nm ± 20 nm) indicated in Fig. 3b), an etching rate ratio of 1.45 ± 0.2 is estimated. The discrepancy between this value and the ratio calculated from the etching rate analysis may be mainly attributed to uncertainties in total layer thickness. This emphasizes the importance of the in-situ tracking as it allows precise detection of the starting point of the ITO etching and calculation of the required etching time irrespective of the actual imprint resist thickness.

By repeating the imprint and etching process rotating the imprint template by an angle for each imprint step, we obtain two-dimensional greyscale patterns in the ITO. In order to determine the etching time for subsequent patterning steps, the existing nanograting has to be taken into account. During coating, the imprint resist fills the voids of the underlying pattern while partly preserving the structure through the layer. However, application of the imprint template forces a new pattern onto the surface, causing differences in resist thickness, which result from both the existing pattern underneath the resist and the newly imprinted grating. As the etching rate of the imprint resist is higher than the etching rate of the ITO, this effect finally leads to flattening of the existing pattern during successive etching steps. While the flattening may be utilized to easily obtain greyscale features, one can also diminish it by choosing the etching time accordingly. The final shape of the resulting nanopattern is determined by the number of the performed imprint and etching steps as well as the angles in which the imprint templates are applied. One

can simply obtain square pillar patterns by using the same imprint template holding a 1D grating structure and rotating it by 90° for the second imprint step. Other designs (such as rectangular or rhomboid shaped pillars) can be fabricated by using multiple 1D templates with different period lengths or applying the PDMS templates at different angles. Examples for various different greyscale pattern designs fabricated with our method are presented in Fig. 4. The generation of more complex patterns such as isosceles triangles requires more than two imprint steps and therefore exact alignment of the imprint templates. For this work, all alignment was done manually, hence preventing the fabrication of those patterns. However, as alignment precision below 100 nm has been shown to be feasible for NIL[34], we expect our method to be suitable for the generation of arbitrary periodic and aperiodic patterns from appropriate master templates.

Since the generation of complex multi-dimensional patterns from one-dimensional master templates requires multiple imprint and etching steps, exact reproducibility between different samples may be difficult to achieve. We therefore envision the main application of our method to be the fabrication of new master template patterns. Subsequently, one may utilize these master templates for pattern duplication via highly reproducible standard nanoimprint lithography techniques. Generating new variable master templates by nanoimprint lithography and ion beam etching using only one or few existing templates is especially beneficial in cases where greyscale EBL may not be available or not feasible due to size constraints. In order to show the applicability of our method to this workflow, we covered the etched ITO gratings with an anti-sticking layer (BGL-GZ-83) and used them as a mold for PDMS imprint templates. With these PDMS stamps we performed a standard UV-NIL process yielding a nanopatterned layer of imprint resist on a glass substrate, which was coated with a thin silver layer for SEM imaging. A comparison of the employed ITO templates and the resulting imprinted nanopatterns is presented in Fig. 5. Both the one-dimensional grating pattern (a) and the two-dimensional pillar pattern (c) show very good conformity to the period length and grating depth of the templates (b) and (d) confirming that the etched ITO samples can indeed be used as master templates for pattern replication. The imprinted samples exhibit higher surface roughness and less distinct pattern features than the templates. We attribute this mainly to the silver coating on top of the resist and not to be a result of the imprint process itself. This is due to the fact that silver may form rough films especially when deposited at the low rates necessary for the fabrication of very thin layers[35], whereas we did not observe roughening of the pattern during any other imprints using the same template material and imprint resist.

Conclusion

In conclusion, we have demonstrated a method to generate variable two-dimensional greyscale nanopatterns in indium tin oxide using only a one-dimensional nanoimprint master template. The patterning process consists of multiple successive steps of nanoimprint lithography and ion beam etching. Greyscale features are obtainable because we cure and etch the imprint resist after each imprint step allowing individual etch durations for each etching step. Additionally, we employed secondary ion mass spectrometry to track the etching progress and precisely control the etching depth yielding two-

dimensional patterns with variable feature height. The patterns generated by this method can subsequently be used as master templates for reproduction. We demonstrated this workflow by reproducing multiple of our etched patterns using a standard UV nanoimprint lithography technique. Finally, we believe our method to be beneficial for device fabrication and prototyping especially in lab environments where techniques such as greyscale EBL are either not available or not desirable due to cost, time or size constraints.

List Of Abbreviations

AFM: atomic force microscopy

EBL: electron beam lithography

IBE: ion beam etching

ITO: indium tin oxide

NIL: nanoimprint lithography

OLED: organic light emitting diode

OPV: organic photovoltaics

PDMS: polydimethylsiloxane

SEM: Scanning electron microscopy

TOF-SIMS: by time-of-flight secondary ion mass spectrometry

Declarations

Availability of data and materials: All data is available from the authors via a reasonable request.

Competing interests: The authors declare that they have no competing interests.

Funding: The authors acknowledge financial support by Interreg (Project Rollflex, 1_11.12.2014).

Authors' contributions: JB suggested the initial etching process, performed the nanopatterning experiments shown in this work and wrote the manuscript. DY performed the etching rate analysis and etching process optimization. MK prepared the samples before the nanopatterning process and performed the AFM investigations of the patterns. MG proposed the utilization of the etching process for the fabrication of two-dimensional greyscale patterns and was a contributor in writing the manuscript. All authors read and approved the final manuscript

Acknowledgements: Not applicable.

References

1. Tang CW, VanSlyke SA (1987) Organic electroluminescent diodes. Appl Phys Lett 51:913–915
2. Reineke S, Lindner F, Schwartz G, Seidler N, Walzer K, Lüssem B, Leo K (2009) White organic light-emitting diodes with fluorescent tube efficiency. Nature 459:234–238
3. Shaheen SE, Brabec CJ, Sariciftci NS, Padinger F, Fromherz T, Hummelen JC (2001) 2.5% efficient organic plastic solar cells. Appl Phys Lett 78:841–843
4. Li S, Ye L, Zhao W, Yan H, Yang B, Liu D, Li W, Ade H, Hou J (2018) A Wide Band Gap Polymer with a Deep Highest Occupied Molecular Orbital Level Enables 14.2% Efficiency in Polymer Solar Cells. J Am Chem Soc 140:7159–7167
5. Meerheim R, Furno M, Hofmann S, Lüssem B, Leo K (2010) Quantification of energy loss mechanisms in organic light-emitting diodes. Appl Phys Lett 97:253305
6. Furno M, Rosenow TC, Gather MC, Lüssem B, Leo K (2012) Analysis of the external and internal quantum efficiency of multi-emitter, white organic light emitting diodes. Appl Phys Lett 101:143304
7. Mladenovski S, Neyts K, Pavicic D, Werner A, Rothe C (2009) Exceptionally efficient organic light emitting devices using high refractive index substrates. Opt Express 17:7562–7570
8. Möller S, Forrest SR (2002) Improved light out-coupling in organic light emitting diodes employing ordered microlens arrays. J Appl Phys 91:3324–3327
9. Li Y, Kovačič M, Westphalen J, et al (2019) Tailor-made nanostructures bridging chaos and order for highly efficient white organic light-emitting diodes. Nat Commun 10:2972
10. Do YR, Kim Y-C, Song Y-W, Lee Y-H (2004) Enhanced light extraction efficiency from organic light emitting diodes by insertion of a two-dimensional photonic crystal structure. J Appl Phys 96:7629–7636
11. Jeon S, Kang J-W, Park H-D, et al (2008) Ultraviolet nanoimprinted polymer nanostructure for organic light emitting diode application. Appl Phys Lett 92:223307
12. Ishihara K, Fujita M, Matsubara I, Asano T, Noda S, Ohata H, Hirasawa A, Nakada H, Shimoji N (2007) Organic light-emitting diodes with photonic crystals on glass substrate fabricated by nanoimprint lithography. Appl Phys Lett 90:111114
13. Jiang W, Liu H, Yin L, Ding Y (2013) Fabrication of well-arrayed plasmonic mesoporous TiO_2/Ag films for dye-sensitized solar cells by multiple-step nanoimprint lithography. J Mater Chem A 1:6433–6440
14. Geyer U, Hauss J, Riedel B, Gleiss S, Lemmer U, Gerken M (2008) Large-scale patterning of indium tin oxide electrodes for guided mode extraction from organic light-emitting diodes. J Appl Phys 104:93111
15. Riedel B, Hauss J, Geyer U, Guetlein J, Lemmer U, Gerken M (2010) Enhancing outcoupling efficiency of indium-tin-oxide-free organic light-emitting diodes via nanostructured high index layers. Appl Phys Lett 96:243302

16. Choi J, Koh T-W, Lee S, Yoo S (2012) Enhanced light extraction in organic light-emitting devices: Using conductive low-index layers and micropatterned indium tin oxide electrodes with optimal taper angle. Appl Phys Lett 100:233303
17. Kluge C, Rädler M, Pradana A, Bremer M, Jakobs P-J, Barié N, Guttmann M, Gerken M (2012) Extraction of guided modes from organic emission layers by compound binary gratings. Opt Lett 37:2646–2648
18. Fujita M, Ueno T, Ishihara K, Asano T, Noda S, Ohata H, Tsuji T, Nakada H, Shimoji N (2004) Reduction of operating voltage in organic light-emitting diode by corrugated photonic crystal structure. Appl Phys Lett 85:5769–5771
19. Fujita M, Ishihara K, Ueno T, Asano T, Noda S, Ohata H, Tsuji T, Nakada H, Shimoji N (2005) Optical and Electrical Characteristics of Organic Light-Emitting Diodes with Two-Dimensional Photonic Crystals in Organic/Electrode Layers. Jpn J Appl Phys 44:3669–3677
20. Lüder H, Gerken M (2019) FDTD modelling of nanostructured OLEDs: analysis of simulation parameters for accurate radiation patterns. Opt Quantum Electron 51:139
21. Schwab T, Fuchs C, Scholz R, Zakhidov A, Leo K, Gather MC (2014) Coherent mode coupling in highly efficient top-emitting OLEDs on periodically corrugated substrates. Opt Express 22:7524–7537
22. Zhang S, Turnbull GA, Samuel IDW (2014) Highly Directional Emission and Beam Steering from Organic Light-Emitting Diodes with a Substrate Diffractive Optical Element. Adv Opt Mater 2:343–347
23. Polywka A, Tückmantel C, Görrn P (2017) Light controlled assembly of silver nanoparticles. Sci Rep 7:45144
24. Iwahashi T, Yang R, Okabe N, Sakurai J, Lin J, Matsunaga D (2014) Nanoimprint-assisted fabrication of high haze metal mesh electrode for solar cells. Appl Phys Lett 105:223901
25. Kudryashov V, Yuan X-C, Cheong W-C, Radhakrishnan K (2003) Grey scale structures formation in SU-8 with e-beam and UV. Microelectron Eng 67–68:306–311
26. Mohamed K, Alkaisi MM, Blaikie RJ (2007) Fabrication of three dimensional structures for an UV curable nanoimprint lithography mold using variable dose control with critical-energy electron beam exposure. J Vac Sci Technol B Microelectron Nanom Struct Process Meas Phenom 25:2357–2360
27. Mattelin M-A, Radosavljevic A, Missinne J, Cuypers D, Van Steenberge G (2020) Design and fabrication of blazed gratings for a waveguide-type head mounted display. Opt Express 28:11175–11190
28. Piaszenski G, Barth U, Rudzinski A, Rampe A, Fuchs A, Bender M, Plachetka U (2007) 3D structures for UV-NIL template fabrication with grayscale e-beam lithography. Microelectron Eng 84:945–948
29. Hemmati H, Magnusson R (2018) Development of tuned refractive-index nanocomposites to fabricate nanoimprinted optical devices. Opt Mater Express 8:175–183
30. Hansen M, Ziegler M, Kohlstedt H, Pradana A, Raedler M, Gerken M (2012) UV capillary force lithography for multiscale structures. J Vac Sci Technol B 30:31601

31. Schift H (2015) Nanoimprint lithography: 2D or not 2D? A review. Appl Phys A 121:415–435
32. Harrer S, Yang JKW, Berggren KK, Ilievski F, Ross CA (2006) Pattern Generation by Using Multi-Step Room-Temperature Nanoimprint Lithography. In: 2006 Sixth IEEE Conf. Nanotechnol. pp 576–579
33. Jahns S, Bräu M, Meyer B-O, Karrock T, Gutekunst SB, Blohm L, Selhuber-Unkel C, Buhmann R, Nazirizadeh Y, Gerken M (2015) Handheld imaging photonic crystal biosensor for multiplexed, label-free protein detection. Biomed Opt Express 6:3724–3736
34. Glinsner T, Lindner P, Mühlberger M, Bergmair I, Schöftner R, Hingerl K, Schmid H, Kley E-B (2007) Fabrication of 3D-photonic crystals via UV-nanoimprint lithography. J Vac Sci Technol B Microelectron Nanom Struct Process Meas Phenom 25:2337–2340
35. Shibata T, Ikeda H, Nishiyama H, Tawa K, Nishii J (2013) Optimization of Metal Quality for Grating Coupled Surface Plasmon Resonance. Phys Procedia 48:179–183

Figures

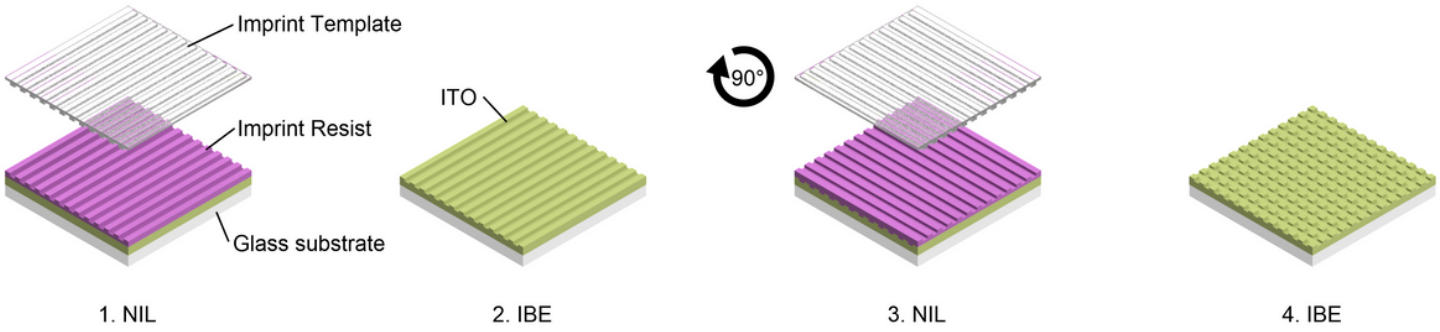

Figure 1

Overview over the nanopatterning process workflow. Multiple steps of nanoimprint lithography and ion beam etching lead to a multi-dimensional nanopattern with variable feature height.

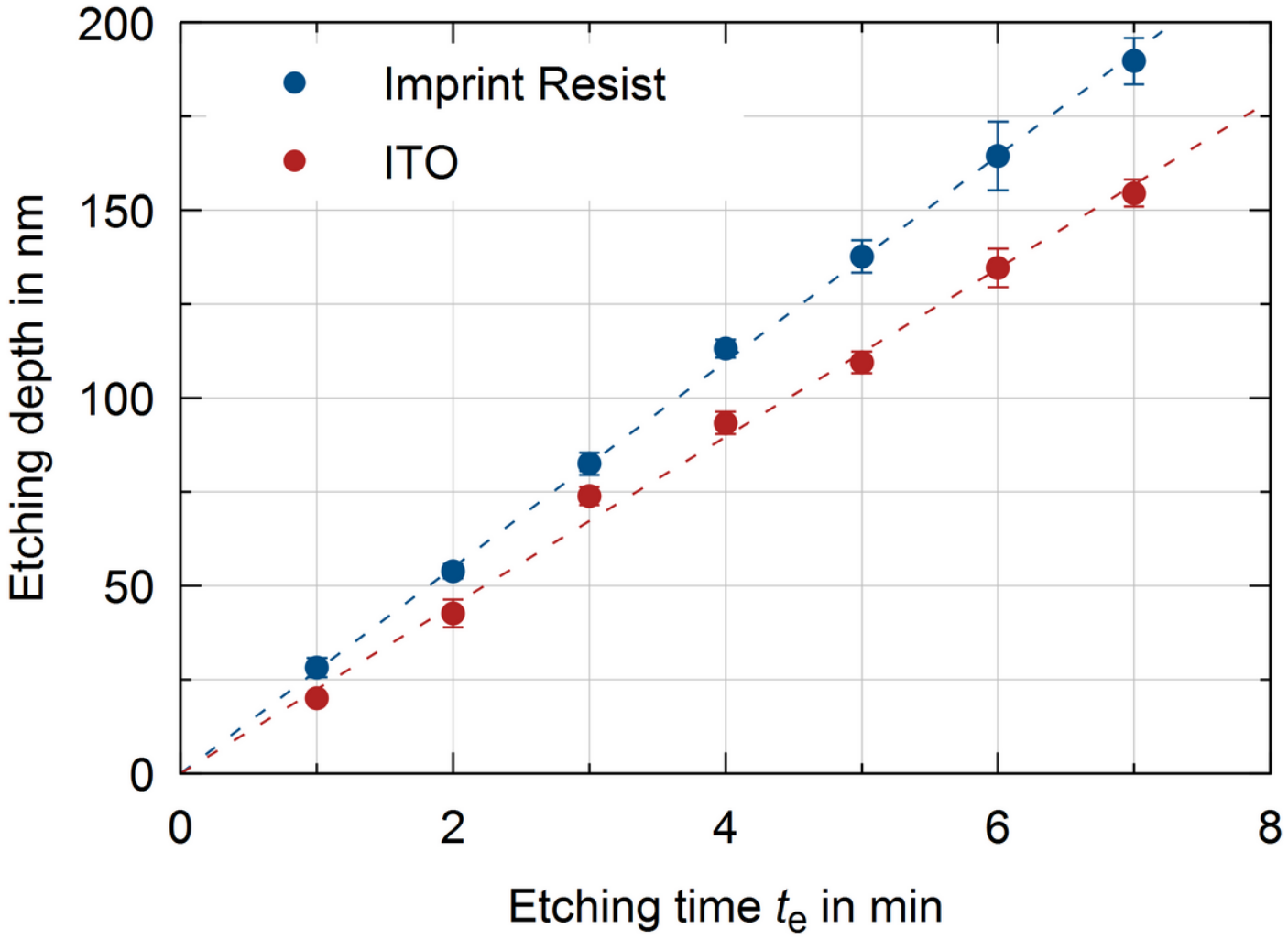

Figure 2

Etching depth on planar samples coated with ITO and imprint resist. The resulting etching rates are 27.4 nm/min for the imprint resist and 22.4 nm/min for the ITO coating.

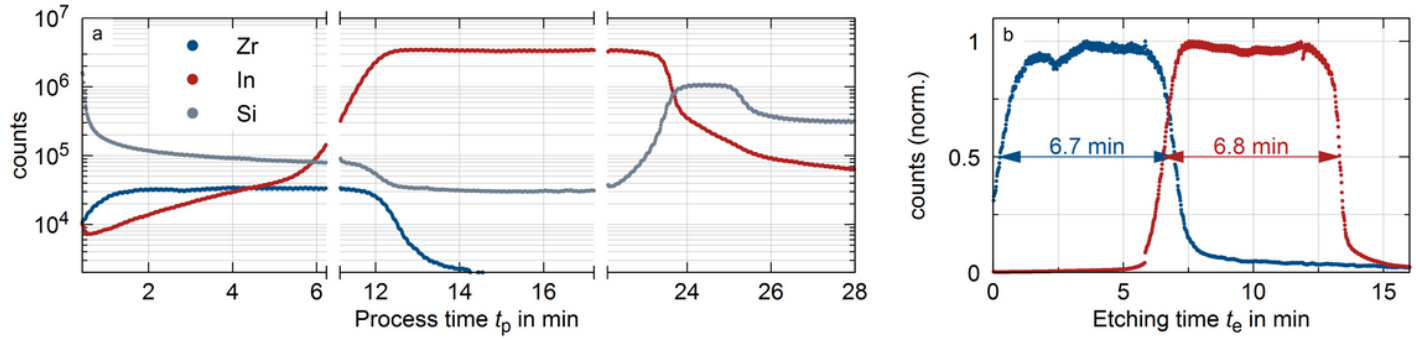

Figure 3

(a) Representation of the complete etching process by TOF-SIMS. Zr counts correspond to etching of the imprint resist whereas In counts correspond to etching of ITO. Si counts correspond to both etching of the

imprint resist and the glass substrate as well as a SiO2 passivation layer underneath the ITO coating. Cooling phases of 4 min are introduced after 6 min of etching to avoid thermal damaging of the samples. (b) We assume the total etching time required for complete removal of the individual layers to be close to the full width at half maximum of the corresponding ion count.

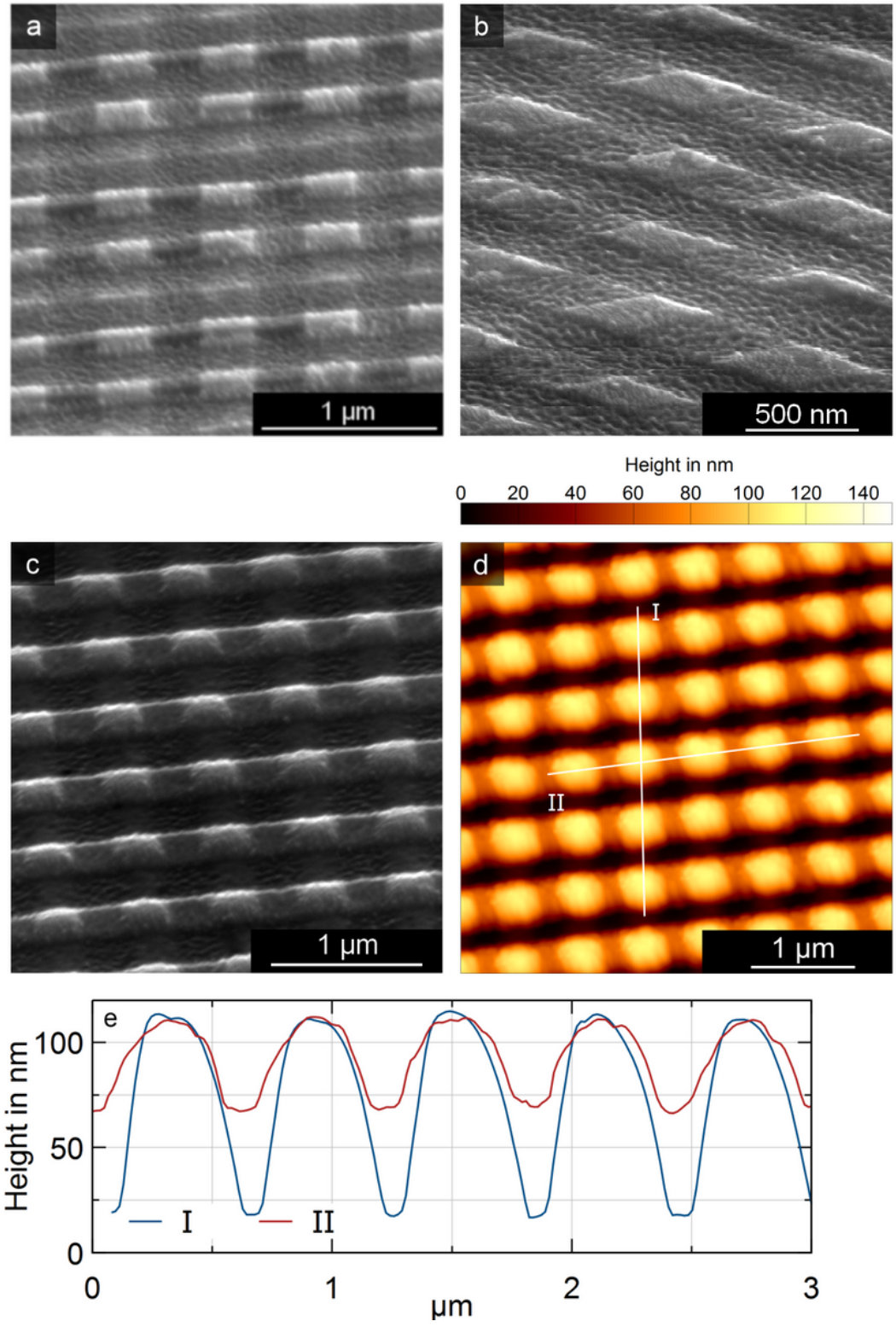

Figure 4

Scanning electron microscopy (SEM) images of greyscale two-dimensional nanopatterns fabricated with the method described above: (a) rectangular pillar pattern with period lengths 400 nm and 600 nm, (b) rhomboid pillar pattern with period length 500 nm at a 40° angle, (c) square pillar pattern with period length 600 nm. (d, e) Atomic force microscopy (AFM) measurement of the pattern depicted in (c). The grating depth along grating directions I and II is approximately 90 nm and 40 nm respectively.

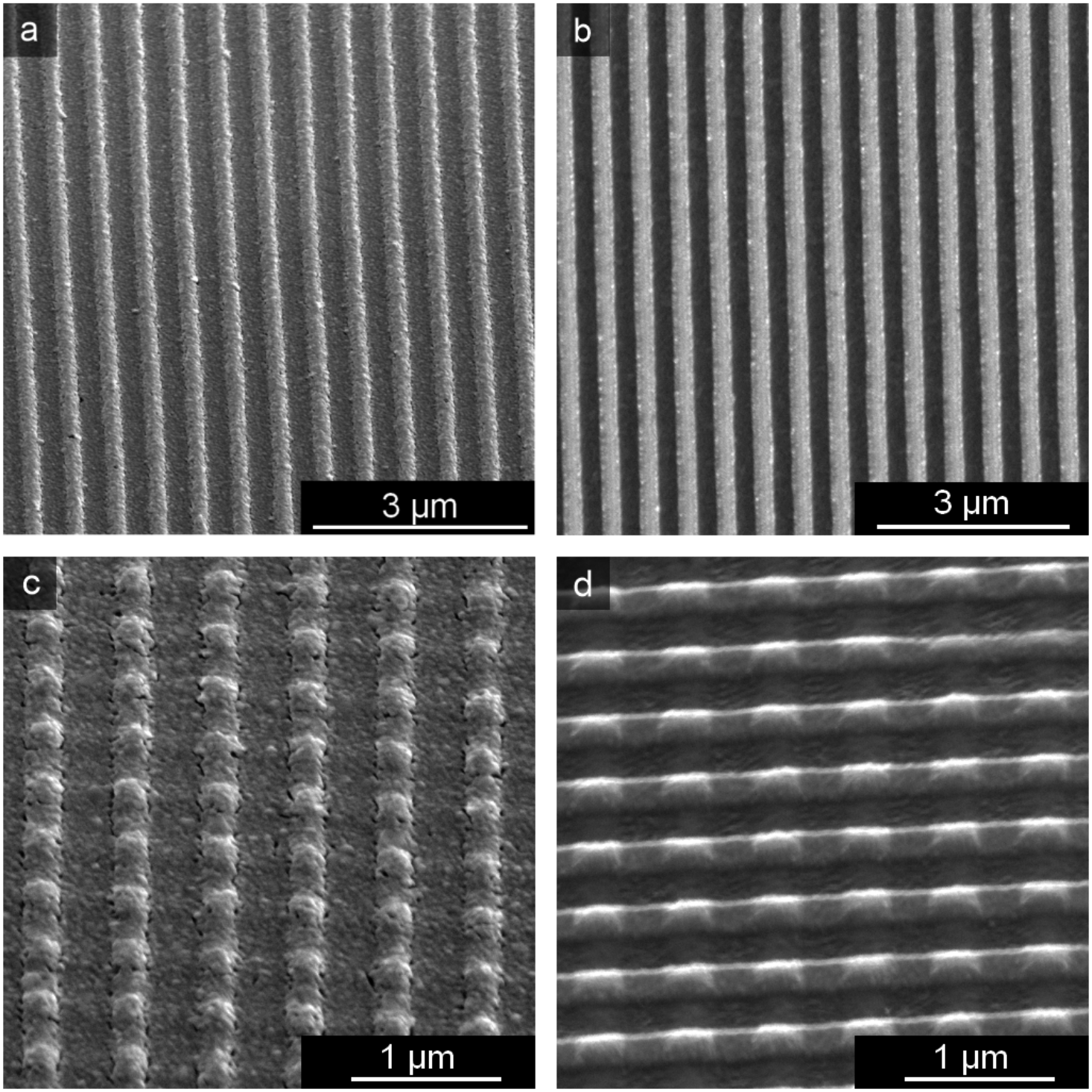

Figure 5

Comparison of imprinted resist coated with a thin Ag layer for SEM imaging (left side) and etched ITO imprint templates (right side): (a, b) one-dimensional grating pattern with period length 600 nm. (c, d) square pillar pattern with period length 600 nm.